Supplementary Information Appendix: Supplementary Figures, Tables and Video descriptions

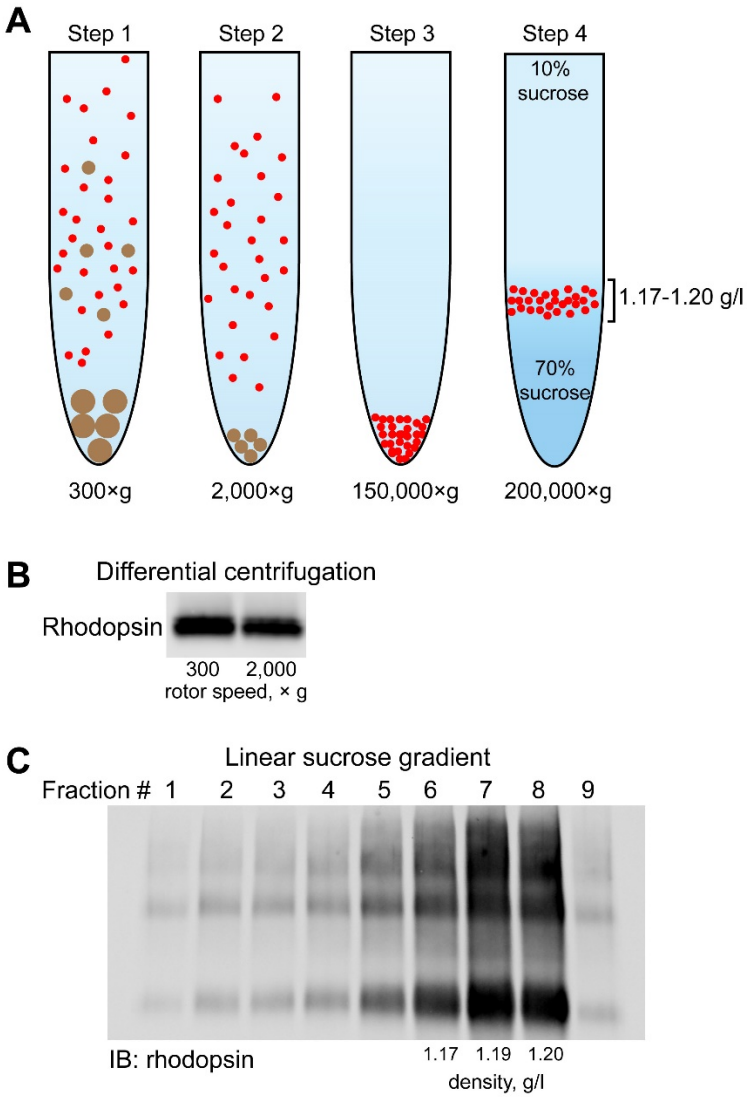

Fig. S1. (A) An illustration of the ectosome purification procedure. Ectosomes were washed from the subretinal space of P14 *rds* mice in Ringer's solution. In *step 1*, this suspension was centrifuged at 300×g and the pellet containing large retinal debris (brown circles) was discarded. In *step 2*, the supernatant from step 1 containing the ectosomes (red circles) was centrifuged at 2,000×g to remove smaller debris. In *step 3*, the supernatant was centrifuged at 150,000×g to sediment ectosomes. In *step 4*, the ectosome-containing pellet was resuspended in PBS and loaded on top of a 10-70% linear sucrose gradient, centrifuged at 200,000×g and the ectosomes were collected from gradient fractions corresponding to a density of 1.17-1.20 g/l. **(B)** Rhodopsin-containing ectosomes remained in suspension upon centrifugation at 300× and 2,000×g in the first two steps of their purification procedure. Rhodopsin content in equal volume (30 µl) aliquots was determined by Western blotting with 1D4 anti-rhodopsin antibody. **(C)** Rhodopsin immunoblotting in fractions isolated from the 10-70% linear sucrose gradient. Fractions 6-8, representing the rhodopsin peak and corresponding to density 1.17-1.20 g/l, were pooled for subsequent analysis.

www.pnas.org/cgi/doi/10.1073/pnas.1913518117

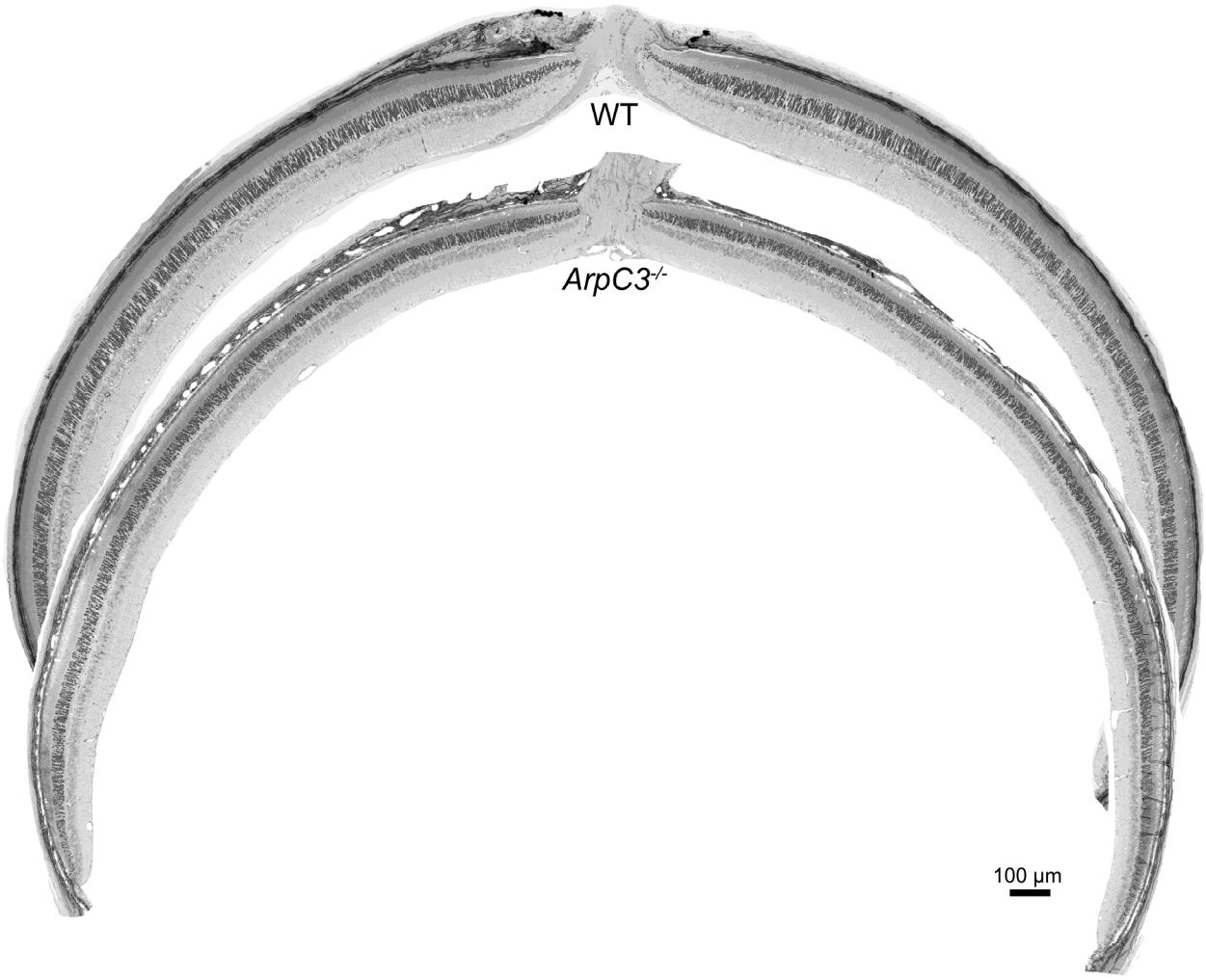

Fig. S2. Representative tile scanned light microscope images of entire fixed retinal sections cut through the optic nerve of P60 WT and P60 *ArpC3*$^{-/-}$ mice.

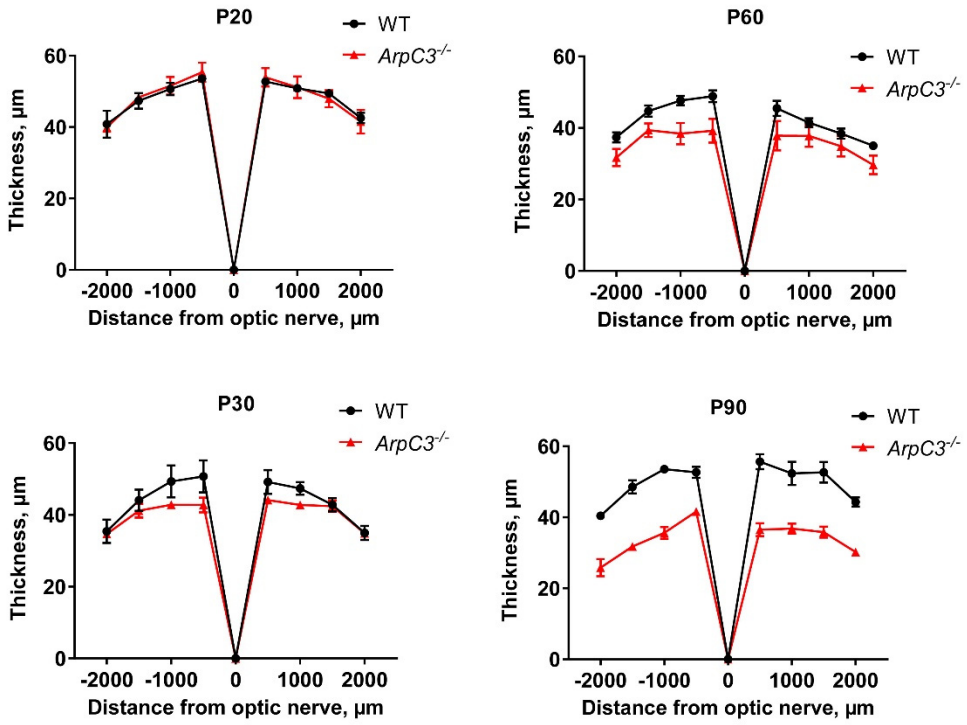

Fig. S3. Spider diagrams showing the outer nuclear layer thickness at 500 µm intervals from the optic nerve head of WT and *ArpC3*$^{-/-}$ mice at the indicated ages. Each data point is shown as mean ± SD. Retinas from at least three mice representing each genotype and age were used for quantification.

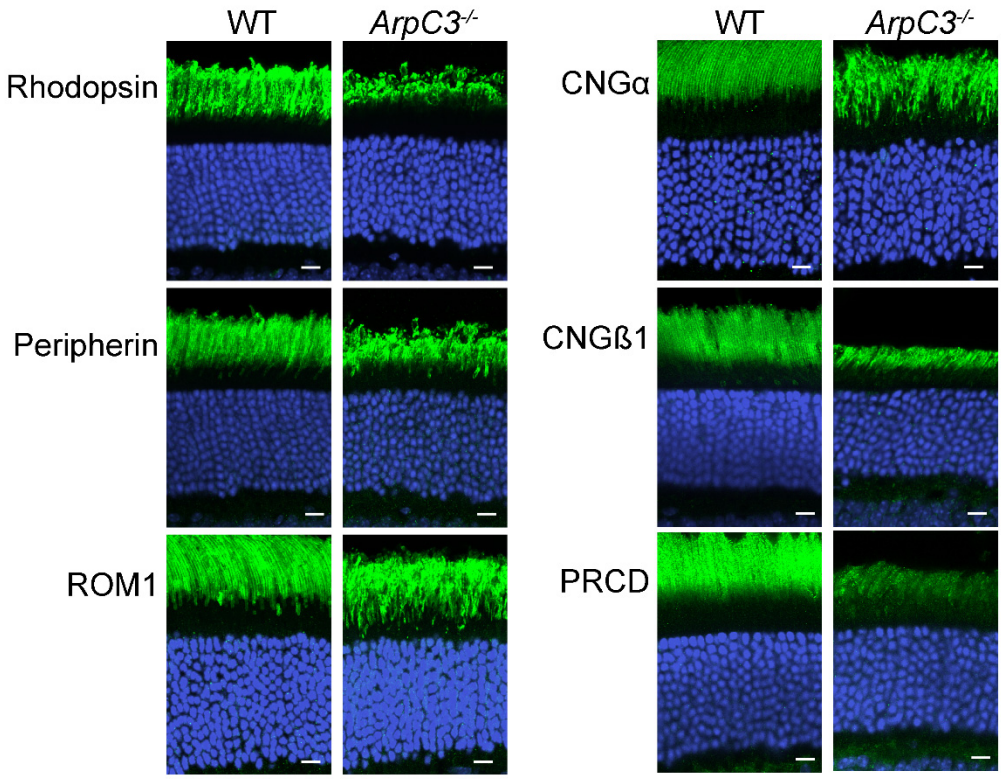

Fig. S4. Immunofluorescent localization of various outer segment proteins (green) in WT and *ArpC3*$^{-/-}$ retinal cross sections at P60. Nuclei are stained by Hoechst (blue). Scale bars are 10 µm.

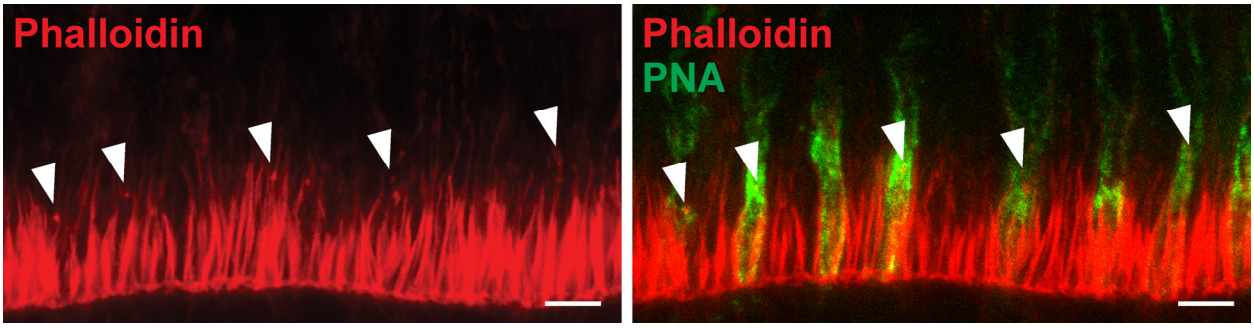

Fig. S5. A retinal cross section from a P60 *ArpC3*$^{-/-}$ mouse co-stained with Alexa Fluor-labeled phalloidin (red) and Alexa Fluor-labeled peanut agglutinin (PNA; green) to label F-actin and cone photoreceptors, respectively. Arrows denote actin puncta present at the base of cone photoreceptor outer segments. Scale bars are 5 µm.

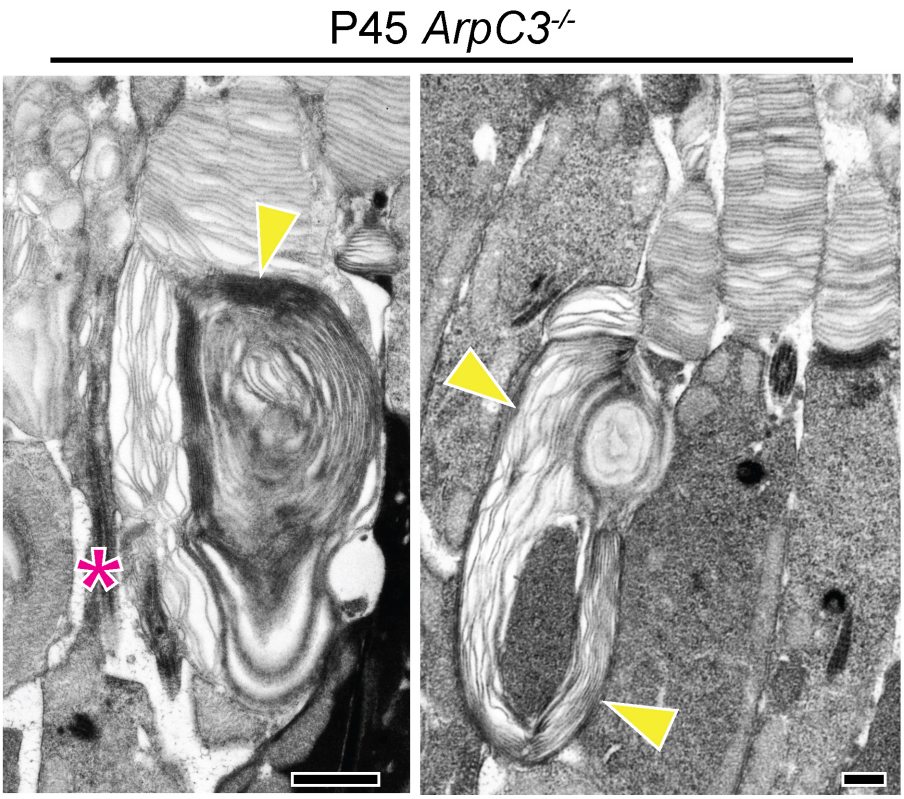

Fig. S6. Electron micrographs of photoreceptor outer segments containing overgrown nascent disc membranes from *ArpC3*$^{-/-}$ mice at P45. Retinal sections were contrasted with tannic acid to discern disc membranes exposed to the extracellular space (darkly stained membranes) from those sequestered inside the outer segment (lightly stained membranes). Overgrown nascent discs are marked by yellow arrowheads. The connecting cilium in the left panel is marked by an asterisk (magenta). Scale bars are 500 nm.

Supplementary Table 1. Proteins confidently identified by mass spectrometry of the ectosomes purified from the subretinal space of *rds* mice. As a control, the ectosome purification procedure and mass spec analysis were performed in parallel using WT mice. Proteins included in the table were identified in both independent experiments and were represented by at least two unique peptides in one of the experiments. There were two independent experiments, one with two technical LC-MS/MS repeats and another with three technical repeats. The data shown for each independent experiment include: 1) the number of unique peptides identified for each protein, 2) the protein confidence score representing the sum of all unique peptide confidence scores for each protein and 3) the total ion intensity representing the sum of all unique peptide ion intensities for each protein. Outer segment proteins are highlighted in green, and proteins related to actin dynamics in yellow.

Supplementary Table 2. A list of ectosome-enriched proteins confidently identified by mass spectrometry. Proteins included in this table were enriched at least two-fold in the material collected from *rds* mice vs. the WT control mice in both independent experiments. The enrichment was calculated based on the ratio of total ion intensity for each protein between *rds* and WT samples. The data shown for each protein include: 1) average confidence scores across all mass spec runs, 2) the total number of unique peptides identified across all mass spec runs, 3) total ion intensity averaged across mass spec runs for *rds* and WT samples, 4) the enrichment between *rds* and WT protein ion intensities averaged between the two independent experiments.

Supplementary Video 1. Video showing 3D reconstruction of the STED confocal image taken at the inner-outer segment junction of a WT mouse (Fig. 1A), in which F-actin is stained with phalloidin (red).

Supplementary Video 2. The video displays, frame by frame, a 3D tomogram of a membrane whorl produced by a rod of P60 *ArpC3*$^{-/-}$ mice. Tomography was conducted in STEM mode on two consecutive ~800 nm-thick retinal sections. Each video frame represents an ~2 nm-thick retinal volume. The magnification is 28,500×, the total volume is 2.1 µm × 2.1 µm × 1.5 µm.

Supplementary Video 3. The video displays, frame by frame, a 3D tomogram of a membrane whorl apparently produced by more than a single rod of P60 *ArpC3*$^{-/-}$ mice. Tomography was conducted in STEM mode on three consecutive ~800 nm-thick retinal sections. Each video frame represents an ~6 nm-thick retinal volume. The magnification is 10,000×, the total volume is 6.32 µm × 7.5 µm × 2.5 µm.

Supplementary Video 4. A video showing a 3D rendering of the segmented tomogram, shown in Supplementary Video 3, of a membrane whorl present in a P60 *ArpC3*$^{-/-}$ mouse retina. The following membranes are highlighted: overgrown and whorled disc membranes (green), inner segment membranes (blue), ciliary membranes (red) and mitochondrial membranes (white).